Input-Specific Spine Entry of Soma-Derived Vesl-1S Protein Conforms to Synaptic Tagging

Daisuke Okada, *et al.*

Science **324**, 904 (2009);
DOI: 10.1126/science.1171498

Science (print ISSN 0036-8075; online ISSN 1095-9203) is published weekly, except the last week in December, by the American Association for the Advancement of Science, 1200 New York Avenue NW, Washington, DC 20005.

Input-Specific Spine Entry of Soma-Derived Vesl-1S Protein Conforms to Synaptic Tagging

Daisuke Okada,* Fumiko Ozawa, Kaoru Inokuchi*

Late-phase synaptic plasticity depends on the synthesis of new proteins that must function only in the activated synapses. The synaptic tag hypothesis requires input-specific functioning of these proteins after undirected transport. Confirmation of this hypothesis requires specification of a biochemical tagging activity and an example protein that behaves as the hypothesis predicts. We found that in rat neurons, soma-derived Vesl-1S (Homer-1a) protein, a late-phase plasticity-related synaptic protein, prevailed in every dendrite and did not enter spines. *N*-methyl-D-aspartate receptor activation triggered input-specific spine entry of Vesl-1S proteins, which met many criteria for synaptic tagging. These results suggest that Vesl-1S supports the hypothesis and that the activity-dependent regulation of spine entry functions as a synaptic tag.

Synaptic plasticity is central for higher brain functions, including memory. Persistent late-phase synaptic plasticity depends on transcription and translation of new gene products, namely plasticity-related proteins (PRPs) or plasticity factors (*1*). Although the mechanisms underlying input-specific functioning of PRPs in the synapses expressing early-phase plasticity are critical for input-specific late-phase plasticity and consistent maintenance of network functions, they are not yet fully understood.

A synaptic tag is a hypothetical mark present in synapses expressing early-phase plasticity; it allows PRPs to function only in the tagged synapses (*2*, *3*), although its molecular identity remains elusive. Three characteristics of a synaptic tag have been pointed out (*4*): A synaptic tag is locally activated, persists with a lifetime of 1 to 4 hours, and interacts with cell-wide molecular events that occur after strong stimulation evokes late plasticity. However, these characteristics are insufficient to define the biochemical activity required for synaptic tagging. It is also critical to specify the cell-wide molecular events that interact with the synaptic tag.

Local synthesis—the activity-dependent translation of some PRPs from mRNAs that reside in nearby dendrites—is a possible mechanism for synaptic tagging (*4*). Local synthesis is involved in long-term facilitation in *Aplysia* (*3*) and supplies several proteins that play important roles in synaptic plasticity in rodents, such as Arc/Arg3.1, PKMζ, and GluR1 (*5*–*8*). However, this mechanism neither happens in a cell-wide manner nor considers the contribution of soma-derived PRPs. On the other hand, although contribution of soma-derived PRPs was suggested in synaptic tagging in the rodent hippocampus (*2*), no soma-derived protein has so far been identified as a PRP consistent with the synaptic tag hypothesis. We sought to identify such a PRP as an example of the synaptic tagging mechanism and to specify cell-wide events that interact with the synaptic tag for soma-derived PRPs.

Previous synaptic tagging studies have primarily been conducted with two-pathway experiments to detect associative late-phase plasticity (*2*). Late-phase plasticity involves several elementary steps: a preceding early phase, induction of PRP synthesis, transport, integration, and synaptic function of PRPs. Identifying a synaptic tagging process among these steps by only measuring the eventual consequence [e.g., changes in transmission (*2*) or synaptic GluR1 accumulation (*9*)] would be difficult. However, these experiments suggest that new PRPs are transported from the soma along dendrites without a predetermined destination (*2*, *10*). Enhanced PRP synthesis facilitated associative late-phase plasticity (*11*), whereas reduced PRP synthesis resulted in competitive maintenance of late-phase plasticity (*12*). These observations suggest that PRP delivery to synapses plays a key role in synaptic tagging.

It is reasonable to assume that a PRP can affect synaptic transmission only after it is delivered to and integrated into the active postsynaptic loci. Material transport across the spine neck is restricted (*13*) and is regulated in an activity-dependent manner for several proteins (*14*–*17*). Thus, we hypothesized that activity-dependent regulation of spine entry of the soma-derived PRPs serves as a synaptic tag (fig. S1), and we tested whether the spine entry has the following features of synaptic tagging: (i) The entry is activity-regulated; namely, PRPs stay in dendrites unless proper activity is provided. (ii) Inputs that activate early-phase plasticity evoke the entry (*2*). (iii) The entry is input-specific (*4*). (iv) PRPs during the dendritic transport from soma are subject to the entry (*2*). (v) The activation of spine entry is independent of protein synthesis (*2*). (vi) The entry activation has a persistent lifetime (*18*). We monitored the spine entry of fluorescent protein–fused Vesl-1S (Homer-1a), a synaptic protein synthesized in the soma during late-phase long-term potentiation (*19*, *20*) and required for long-term fear memory (*21*, *22*).

Spine entry of Vesl-1S protein. Enhanced green fluorescent protein (EGFP)–tagged Vesl-1S (VE) or EGFP alone was exogenously expressed in dissociated primary culture of rat hippocampal neurons (fig. S2) (*23*). The replacement of extracellular medium with magnesium-free artificial cerebrospinal fluid (Mg-free ACSF) for 10 min led to the activation of synaptic *N*-methyl-D-aspartate (NMDA) receptors via glutamatergic transmission by spontaneous firing (*24*). VE fluorescence in mushroom-type spines was further observed in normal ACSF for 4 hours, and its increase relative to prestimulus intensity (F/F_{pre}) was calculated. VE fluorescence intensity increased gradually over time (Fig. 1A) in some but not all spines, which reflects heterogeneous inputs from spontaneous firing (Fig. 1B) (*22*), whereas changes in spine shape and size were more modest. To evaluate changes in a small portion of spines, we introduced a trap index: a numerical indication of VE increase in spines expressed as a rightward shift of cumulative frequency curves (Fig. 1C). Mg-free ACSF triggered a persistent and gradual increase in the trap index (Fig. 1D). The average trap index 240 min after the onset of stimulation (final trap index) was 2.08 ± 0.23 (SD) ($N = 7$ cells), which was significantly larger ($P = 2.1 \times 10^{-4}$, *t* test) than that measured in unstimulated neurons (1.41 ± 0.10, $N = 5$ cells). Mg-free ACSF did not increase fluorescence in spines of neurons expressing only EGFP (final trap index = 1.42 ± 0.17, $N = 4$ cells; $P = 0.001$ versus VE, *t* test).

To specify how spine fluorescence increased after stimulation, we estimated passive entry associated with size enlargement by line-scan analysis of individual spines. The analysis indicated that Mg-free stimulation largely increased the peak intensity [before stimulation: 8.8 ± 4.2 AU (arbitrary units); 4 hours after stimulation: 15.2 ± 7.1 AU; $N = 74$ spines from six cells, $P = 5.3 \times 10^{-10}$, *t* test] (Fig. 1E), whereas spine size (head half-width) was not affected (1.1 ± 0.4 μm versus 1.2 ± 0.4 μm, $P = 0.094$, *t* test) (Fig. 1F). Although the spine enlargement associated with long-term potentiation is greater in initially smaller spines (*25*), increases in the peak intensity and initial size were not correlated ($r = -0.14$), which suggests that the VE increase in spines is independent of morphological plasticity (Fig. 1G).

Incubation with a protein synthesis inhibitor, cycloheximide (CHX), did not affect the VE increase after Mg-free stimulation (final trap index = 2.00 ± 0.25, $N = 5$; $P = 0.62$, *t* test) (Fig. 1H). VE content was not affected by incubation with 5 μM *clasto*-lactacystin β-lactone (LCL), a specific inhibitor of proteasomal activity involved in Vesl-1S protein degradation (*26*) (final trap index = 2.02 ± 0.10, $N = 3$; $P = 0.42$, *t* test) (Fig. 1I). Together, these results indicate that the activity-dependent spine entry of the VE

Mitsubishi Kagaku Institute of Life Sciences (MITILS), 11 Minamiooya, Machida, Tokyo 194-8511, Japan, and Japan Science and Technology Agency (JST), Core Research for Evolutional Science and Technology (CREST), 4-1-8 Honcho, Kawaguchi 332-0012, Japan.

*To whom correspondence should be addressed. E-mail: kaoru@mitils.jp (K.I.); dada@mitils.jp (D.O.)

protein, but not synthesis or degradation, increases the VE content in spines. Henceforth, we call this activity VE trapping.

VE trapping is input-specific. Microperfusion was used to test the input specificity of VE trapping. Rhodamine was co-applied to estimate the affected area and to confirm whether the microperfusion reached the cell surface (Fig. 2, A and B). Microperfusion of normal ACSF did not affect VE fluorescence in spines, both inside and outside of the perfusion area (Fig. 2, C to E). Under these conditions, the increase in spine VE fluorescence followed a normal distribution in both areas as assessed by χ^2 analysis. This enabled comparison using a *t* test, which showed no significant difference between the areas (table S1); thus, microperfusion does not affect the spine fluorescence by nonspecific factors such as influx impact.

In contrast, local stimulation with Mg-free ACSF containing NMDA and glycine caused VE trapping exclusively inside the microperfusion area. The χ^2 analysis detected a significant deviation of VE increase from the normal distribution inside the perfusion area of three cells (Fig. 2, F to H, fig. S3, and cells 1 to 3 in table S1), but not outside the area. We applied a *t* test to the remaining five cells (cells 4 to 8 in table S1), for which spine fluorescence intensity was estimated as a normal distribution by χ^2 analysis, and found a significantly larger VE trapping inside the perfusion area than outside (Fig. 2, I to K).

When Mg-free ACSF containing NMDA, glycine, and 40 μM MK801 (an irreversible open-channel blocker specific to NMDA receptors) was used for microperfusion, VE trapping was not detected either inside or outside the stimulated area (Fig. 2, L to N, and table S1), which indicates that VE trapping is NMDA receptor–dependent. Bath application of Mg-free ACSF after microperfusion with Mg-free ACSF containing NMDA, glycine, and MK801 led to VE trapping in spines outside of the microperfusion (Fig. 2, O to Q, and table S1), whereas spines treated with MK801 did not exhibit VE trapping.

VE stays in the dendrite unless NMDA receptors are activated. The promoter region of our VE plasmid is activated by 0.02 mM forskolin and 0.1 mM 3-isobutyl-1-methylxanthine (FI) (fig. S4) (*27*). VE fluorescence significantly increased in dendrites after bath perfusion of FI (Fig. 3, A to D). F/F_{pre} 240 min after FI application (1.10 ± 0.01, N = 6 cells) was significantly larger than that without stimulation (0.98 ± 0.04, N = 6 cells; P = 0.011, *t* test), whereas Mg-free ACSF did not increase dendritic VE fluorescence (F/F_{pre} 240 min after Mg-free ACSF application = 0.99 ± 0.04, N = 6 cells; P = 0.83 versus ACSF, *t* test) (Fig. 3E). In contrast, VE fluorescence in spines was not significantly affected by FI treatment alone (trap index 240 min after FI = 1.63 ± 0.21, N = 5; P = 0.008 versus Mg-free, P = 0.071 versus ACSF, *t* test) (Fig. 3, F to L). Sequential treatment of cells with FI followed by Mg-free ACSF enhanced VE trapping (P = 0.029 versus Mg-free, *t* test) (Fig. 3L). Similar results were obtained using BrcG [8-bromo-cGMP (guanosine 3′,5′-monophosphate)] instead of Mg-free ACSF

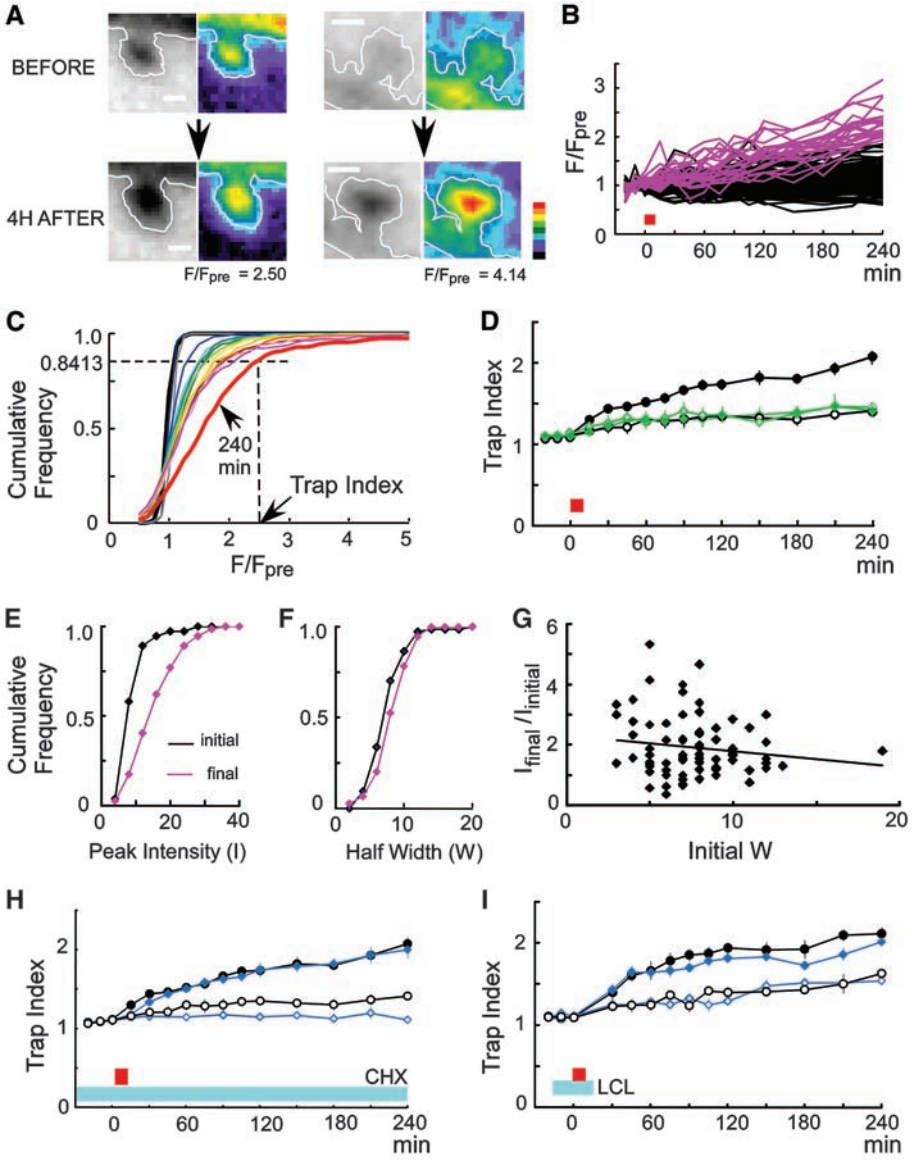

Fig. 1. VE trapping in spines. (**A**) VE fluorescence images in spines before and 4 hours after stimulation in both inverted black-and-white (black is higher) and pseudocolors (both scales apply to similar images in later figures). Scale bars, 1 μm. (**B**) Changes by Mg-free ACSF stimulation (red rectangle) in fluorescence intensity (*F*) compared with prestimulus (F_{pre}) in 121 individual spines of a neuron. Magenta lines show 24 spines with F/F_{pre} values at 240 min that are greater than the average + SD (1.39 + 0.53 = 1.92). (**C**) Cumulative frequency curves of the pooled data of 652 spines in seven Mg-free stimulated neurons. Line colors indicate time (black, 20 min before; gray, 10 min before; dark blue, immediately before; blue, 15 min after; pale blue, 30 min after; dark green, 45 min after; green, 60 min after; yellow-green, 75 min after; yellow, 90 min after; dark yellow, 115 min after; orange, 120 min after; brown, 150 min after; pink, 180 min after; purple, 210 min after; red, 240 min after stimulation). The definition of trap index is indicated. (**D**) Trap index time courses. Values are averages ± SEM (vertical bars). Solid circles, Mg-free ACSF on VE; solid green diamonds, Mg-free ACSF on EGFP; open circles, VE without stimulation; open green diamonds, EGFP without stimulation. (**E** and **F**) Line-scan analysis of 74 spines from six cells on peak intensity *I* (E) and half-width *W* (F) of spine fluorescence before and 4 hours after Mg-free stimulation. (**G**) Correlation between relative increase in *I* and initial value of *W*. (**H**) Trap index time courses. Solid circles, Mg-free; open circles, without stimulation; solid and open blue diamonds, Mg-free in the presence of 20 μM CHX and CHX alone, respectively. (**I**) Trap index time courses. Solid circles, Mg-free + 0.05% dimethyl sulfoxide (DMSO); solid blue diamonds, Mg-free in the presence of 5 μM LCL; open blue diamonds, LCL alone; open circles, 0.05% DMSO.

(F/F_{pre} 240 min after stimulus = 1.01 ± 0.02, N = 5 cells; P = 0.41 versus ACSF, t test) (Fig. 3, E and L; see below).

Soma-derived Vesl-1S is subject to VE trapping. Vesl-1S mRNA was detected in the soma but not in the dendrites (fig. S5), which suggested that Vesl-1S proteins are synthesized in the soma and subsequently transported to dendrites. Vesl proteins are carried by transport vesicles via the interaction with metabotropic glutamate receptors (mGluRs 1 and 5) (*28*, *29*); therefore, VE proteins during dendritic vesicular transport may be subject to VE trapping. We next examined this possibility with the use of photoactivatable GFP (PAGFP) fused with Vesl-1S (VPA) (*30*). VPA proteins in the soma should be transported to the entire span of the cell along dendrites, and should be trapped in spines in an input-specific manner (Fig. 4A). Initially, cells expressing DsRed2, cotransfected as a morphological marker, showed only a slight fluorescence of VPA in the soma and a total absence of VPA fluorescence in dendrites. Brief photoactivation in the soma led to clear VPA fluorescence in the soma (Fig. 4B). The average photoactivation of VPA was smaller (factor of 5.4 ± 3.1, N = 13) than that of PAGFP alone (factor of 34.1 ± 8.3, N = 4), consistent with the instability of the Vesl-1S protein (*26*). VPA fluorescence moved along every dendritic branch toward the distal ends, and this movement did not require local stimulation (Fig. 4C). Next, the dendritic region was viewed at higher magnification to acquire images before stimulation after somatic photoactivation; subsequently, neurons received microperfusion with normal ACSF 15 to 25 min after photoactivation and were observed for an additional 4 hours (Fig. 4D). VPA progressively increased in every dendrite, but it did not enter spines (Fig. 4, E to G, and table S2).

Local NMDA receptor activation caused VPA trapping inside, but not outside, the microperfusion area in all six cells tested after 4 hours (Fig. 5). A χ^2 analysis revealed significant deviation from normal distribution in two cells (Fig.

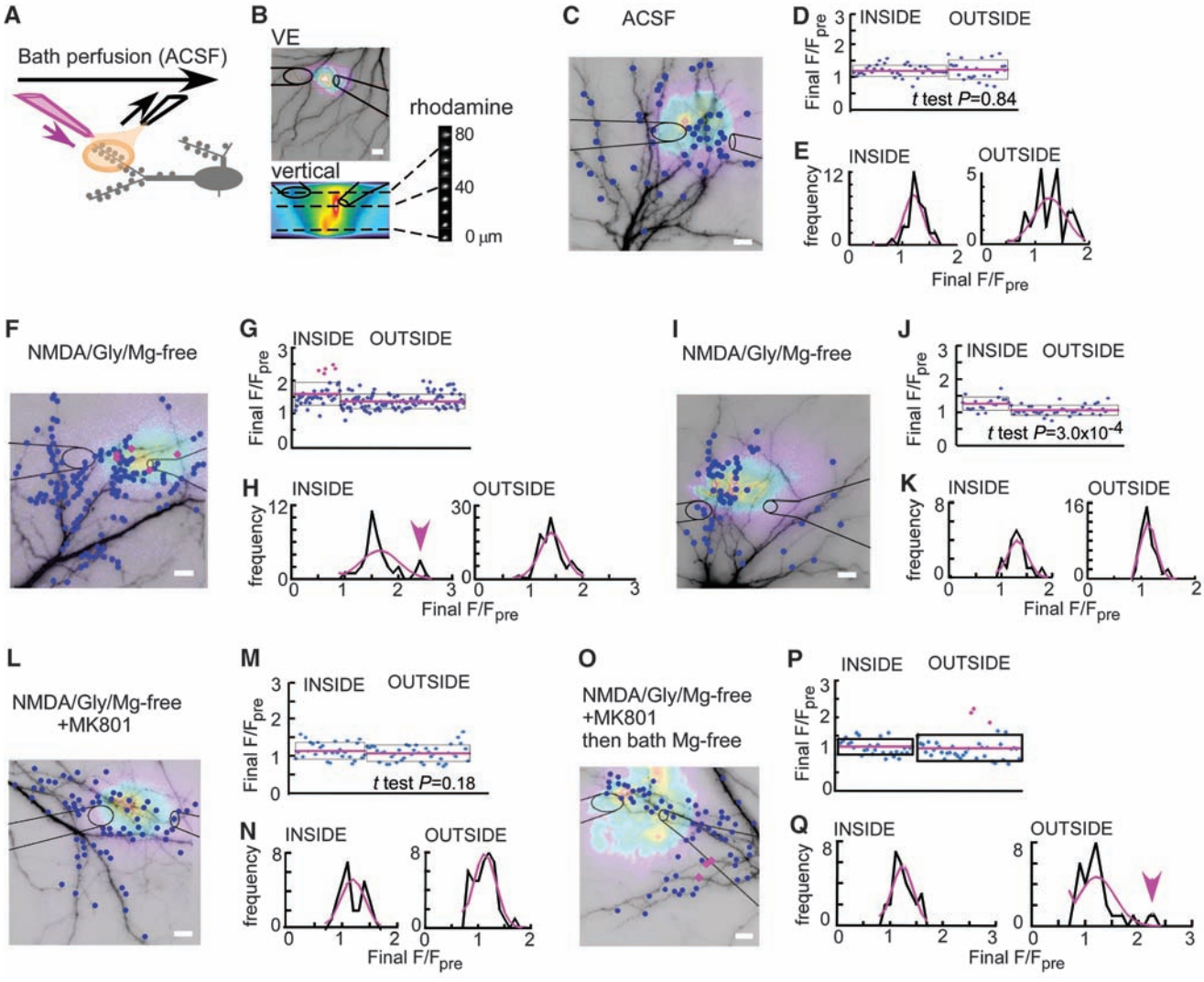

Fig. 2. Input-specific VE trapping. (**A**) Arrangement of injector (magenta) and suction (black) pipettes. (**B**) A vertical view of rhodamine fluorescence was reconstructed in three dimensions from images at different focal planes at 10-μm intervals. A VE fluorescence image in dendrites is superimposed with rhodamine image (pseudocolors) at the height of the target dendrite and pipette positions (black lines). Scale bar, 10 μm. (**C** to **E**) Microperfusion with normal ACSF for 10 min. (C) A representative VE image. Red and blue circles represent spines with significant and nonsignificant VE trapping by χ^2 test 240 min after microperfusion, respectively. Pipette positions and rhodamine distribution (pseudocolors) are superimposed. (D) F/F_{pre} of each spine 240 min after microperfusion. Averages (red line) and average ± 1 SD levels (box) of the inside and outside spines are shown. (E) Frequency distribution of (D) (black) and the normal distribution calculated from the average and the SD (magenta). (**F** to **H**) Local NMDA receptor activation by microperfusion with Mg-free ACSF containing 0.15 mM NMDA and 10 μM glycine for 10 min. Arrowhead in (H) indicates significant deviation in the frequency distribution detected by χ^2 test. (**I** to **K**) Local NMDA receptor activation by microperfusion. A t test showed significantly larger VE tapping in the inside area than outside. (**L** to **N**) Local NMDA receptor activation cocktail with 40 μM MK801. (**O** to **Q**) Bath application of Mg-free ACSF 1 hour after MK801 microperfusion.

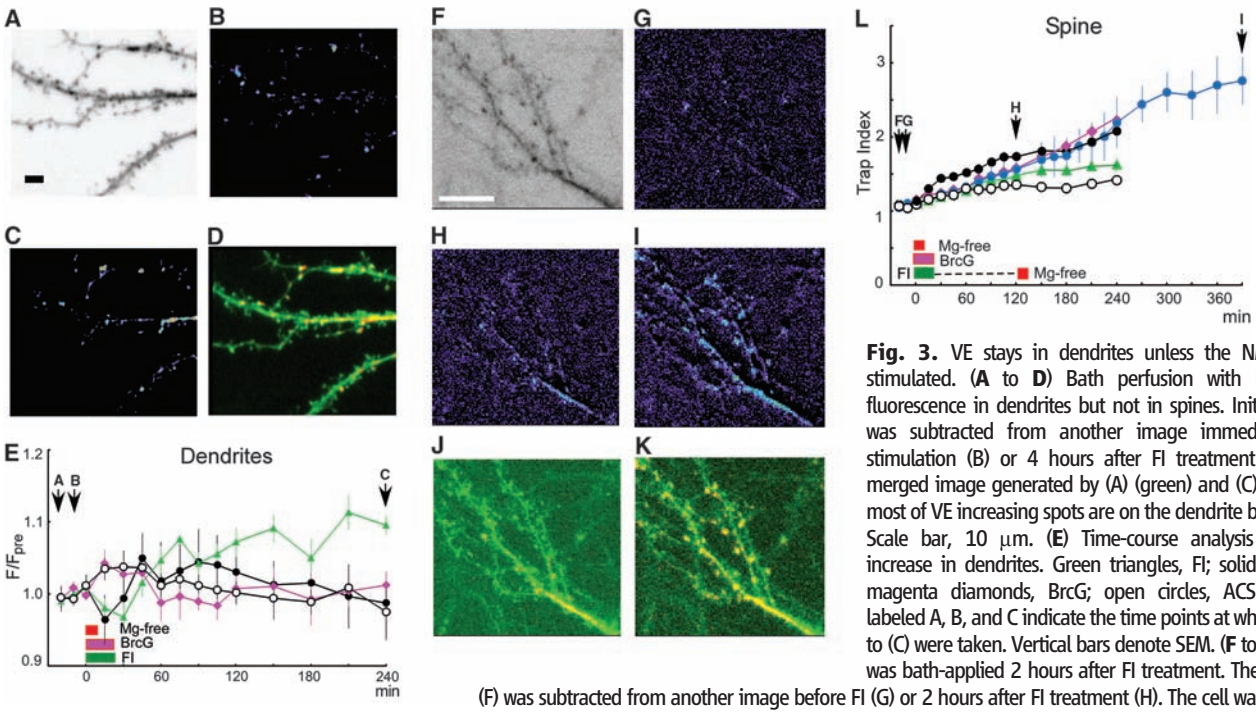

Fig. 3. VE stays in dendrites unless the NMDA receptor is stimulated. (**A** to **D**) Bath perfusion with FI increased VE fluorescence in dendrites but not in spines. Initial VE image (A) was subtracted from another image immediately before FI stimulation (B) or 4 hours after FI treatment (C). In (D), the merged image generated by (A) (green) and (C) (red) shows that most of VE increasing spots are on the dendrite but not the spines. Scale bar, 10 μm. (**E**) Time-course analysis of fluorescence increase in dendrites. Green triangles, FI; solid circles, Mg-free; magenta diamonds, BrcG; open circles, ACSF alone. Arrows labeled A, B, and C indicate the time points at which pictures in (A) to (C) were taken. Vertical bars denote SEM. (**F** to **K**) Mg-free ACSF was bath-applied 2 hours after FI treatment. The initial VE image (F) was subtracted from another image before FI (G) or 2 hours after FI treatment (H). The cell was then stimulated by Mg-free ACSF. Subtraction image (4 hours after Mg-free stimulation minus initial VE image) (I) shows fluorescence increase in spines. (J) The merged image generated by (F) (green) and (H) (red). (K) The merged image generated by (F) (green) and (I) (red). Scale bar, 10 μm. (**L**) Time-course analysis of trap index in spines. Solid blue circles, FI application before Mg-free stimulation; other symbols are as in (E). Arrows labeled F, G, H, and I indicate the time points at which pictures in (F) to (I) were taken.

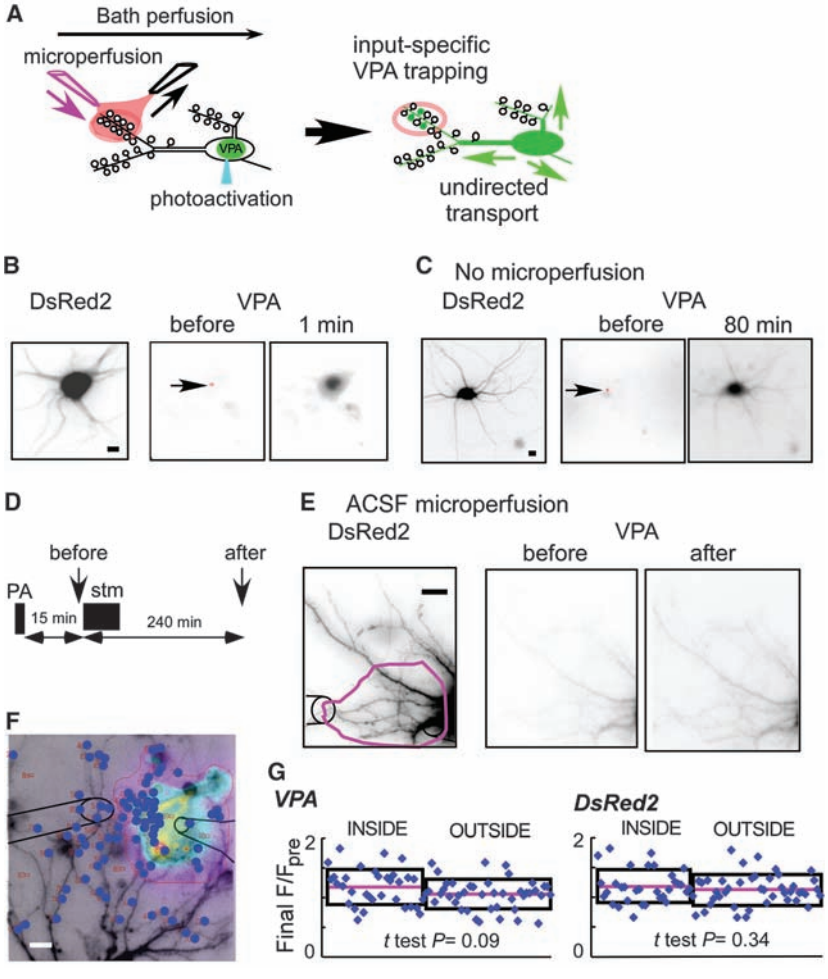

Fig. 4. Somatic VPA spreads cell-wide but does not enter spines. (**A**) Experimental design. VPA in soma was photoactivated by laser illumination (blue arrowhead) and then carried along dendrites (green arrows). Distal dendrites with spines received microperfusion. AlexaFluor633 was used instead of rhodamine. VPA trapping should be exclusive to spines inside the microperfusion area. (**B**) Photoactivation of VPA. A cell expressing DsRed was selected (left) and its PAGFP image (middle) was taken. The entire soma was illuminated with a laser spot (red spot indicated by the arrow) by manual scanning. Both DsRed2 (not shown) and VPA (right) images were taken immediately after photoactivation. (**C**) VPA fluorescence gradually increased in entire dendrites without any stimulation. Scale bar, 10 μm. (**D**) Experimental procedures defining "before" and "after" here and in Fig. 5. PA, photoactivation; stm, microperfusion. (**E**) Microperfusion with normal ACSF for 10 min. Images of DsRed2 (before) and VPA (before and after) are shown. The magenta line encloses the estimated area of stimulation. (**F**) DsRed2 image of dendrites with VE trapping significance (circles), estimated microperfusion area (pseudocolors), and pipette positions. Scale bar, 10 μm. (**G**) The F/F_{pre} value of each spine measured 240 min after microperfusion (see Fig. 2).

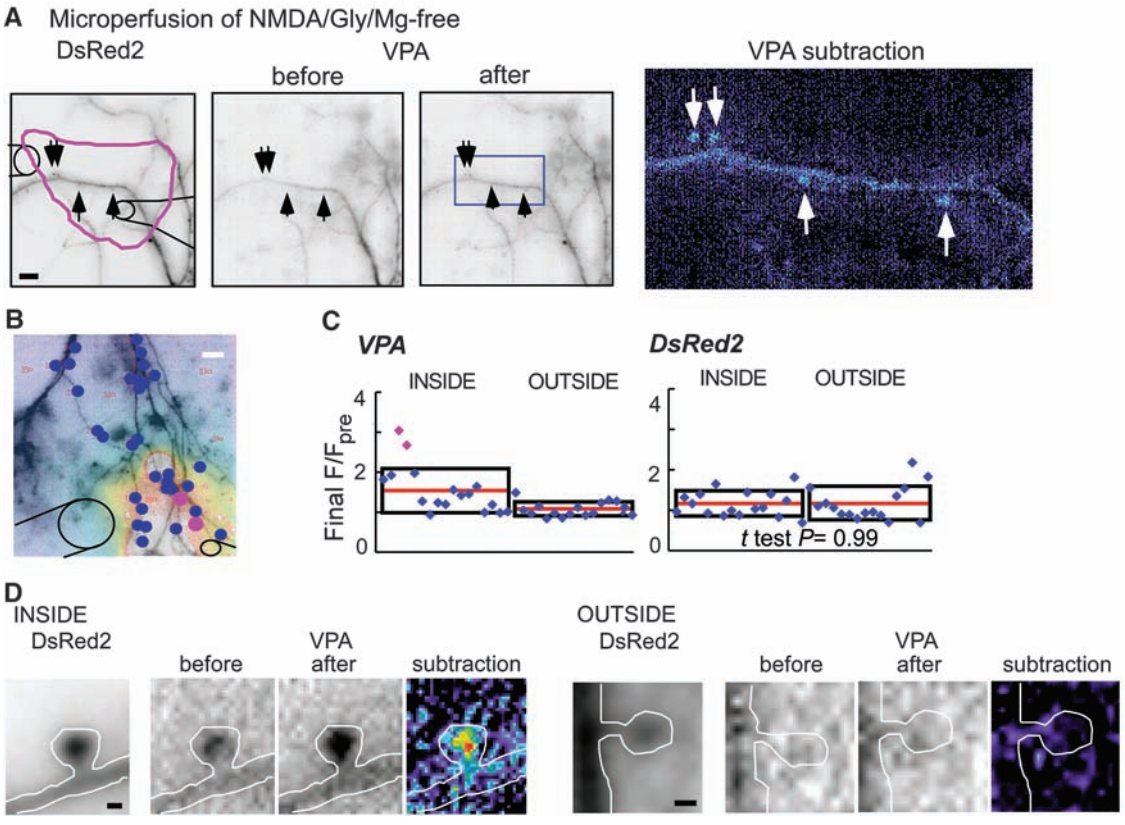

Fig. 5. VPA trapping by local NMDA receptor activation. (**A**) Microperfusion with Mg-free ACSF containing NMDA and glycine for 10 min in a limited area (magenta line) resulted in VPA trapping in some inside spines (arrows). The VPA subtraction image in pseudocolors ("after" minus "before") is shown to magnify the spines in the blue rectangle in the "after" image. Scale bar, 10 μm. (**B**) DsRed2 image of dendrites (another cell) with VE trapping significance (circles), estimated microperfusion area (pseudocolors), and pipette positions. Scale bar, 10 μm. (**C**) F/F_{pre} of each spine measured 240 min after microperfusion. (**D**) Representative images of VPA trapping inside (F/F_{pre} of VPA = 1.96) and outside (F/F_{pre} of VPA = 1.31) spines in a cell. Scale bar, 0.5 μm.

5 and cells 1 and 2 in table S2); a *t* test performed for the remaining four cells (fig. S6 and cells 3 to 6 in table S2) showed that the VPA increase was always significantly greater inside the microperfusion area than outside. The final F/F_{pre} values of VPA and DsRed2 were not correlated (fig. S7). These movements were not observed for PAGFP alone (fig. S8 and table S2). DsRed2 fluorescence in spines was not affected in all experiments (table S2).

We also tested whether spine trapping is affected when dendritic transport of Vesl-1S protein is disrupted. Bath perfusion of Mg-free ACSF did not evoke VE trapping in cells expressing the W24A mutant of Vesl-1S, which does not interact with mGluRs 1 and 5 (*31*) (final trap index = 1.63 ± 0.12, $N = 4$; $P = 0.008$, *t* test) (fig. S9A). VPA transport after local NMDA receptor activation was disrupted when the extracellular medium contained 1 μM colchicine, a microtubule dissociation reagent (fig. S9B).

Signals for VE trapping. Calcium influx through NMDA receptor channels activates neuronal nitric oxide (NO) synthase (*32*). NO in turn increases cGMP, the intrinsic activator of protein kinase G (PKG) (*33*). Extracellular Ca^{2+} ions and the NO-PKG signaling pathway were required for NMDA receptor–dependent VE trapping (fig. S10). We also tested several inhibitors of other signals and found that activation of mGluRs 1 and 5 was not involved in VE trapping (table S3) (*22*).

A membrane-permeable analog of cGMP, BrcG, activated VE trapping (final trap index = 2.14 ± 0.25, $N = 5$ cells; $P = 1.9 \times 10^{-5}$ versus ACSF, *t* test) but did not alter the EGFP spine content (1.42 ± 0.21, $N = 5$ cells; $P = 0.95$ versus ACSF, *t* test) (Fig. 6A). BrcG failed to evoke VE trapping in the presence of 1 μM tetrodotoxin (TTX) throughout the experiment (final trap index = 1.24 ± 0.10, $N = 5$; $P = 7.5 \times 10^{-5}$ versus BrcG, *t* test), whereas 50 nM TTX, which selectively suppresses Na^+ channels in dendrites where the channels are expressed sparsely (*34*, *35*), did not affect VE trapping evoked by BrcG (final trap index = 1.95 ± 0.11, $N = 6$; $P = 0.12$ versus BrcG, *t* test) (Fig. 6A). These results suggest that VE trapping requires a TTX-sensitive factor released by presynaptic activity in addition to NO-PKG signaling.

We used this synergy to estimate the lifetime of the PKG cascade. Cells were stimulated with BrcG in the presence of 1 μM TTX. After further application of TTX for 2 hours, during which VE trapping was not observed, TTX was washed out and VE trapping was measured in normal ACSF for an additional 4 hours. VE fluorescence gradually increased in spines after TTX washout, and the trap index after 4 hours of washout was similar to that achieved without TTX (Fig. 6B). By changing the duration of TTX application, we found that the persistent activity lasted unchanged up to 3 hours, but TTX application for 4 hours abolished the VE trapping ability (Fig. 6, C and D). Interruption of TTX application for 1 hour led to a recovery of VE trapping activity after TTX washout, which was decreased by reapplication of TTX (Fig. 6E). Analysis of the average increase rates during initial TTX treatment (0.001 ± 0.010/min), TTX washout (0.0029 ± 0.019/min), and second application of TTX (0.0006 ± 0.007/min) showed a significant activity increase during the washout period ($P = 0.04$ versus initial TTX, $P = 0.02$ versus second TTX; *t* test) (Fig. 6F).

Discussion. The present study revealed a mechanism of activity-dependent spine sorting for a PRP synthesized in the soma (Vesl-1S): VE trapping. We found that VE trapping meets the six criteria for synaptic tagging: (i) VE proteins did not enter the spines of hippocampal neurons in culture unless cells were properly activated (Fig. 3), which supports our central assumption that spine entry of Vesl-1S is activity-regulated. (ii) VE trapping required NMDA receptor activation, a known trigger of early-phase plasticity (Fig. 2) (*2*). (iii) VE trapping was input-specific (Fig. 2). (iv) VE trapping was independent of protein synthesis (Fig. 1) (*2*). (v) Soma-derived VE proteins were trapped into spines in a manner dependent on the dendritic vesicular transport (Fig. 5) without predetermined destination (Fig. 4), which is the most outstanding feature of synaptic tagging, discriminating it from the mail hypothesis (*10*). (vi) VE trapping was persistently permitted when PKG downstream signals were active (Fig. 6) (*22*).

On the basis of these results, we propose that Vesl-1S protein is a PRP that behaves in a manner consistent with the synaptic tag hypothesis. We conclude that activity-dependent PRP trapping in spines conforms to the synaptic tag hypothesis (Fig. 6G). The trapped PRPs should be further carried from the spine neck to synaptic membranes or other parts of the machinery that

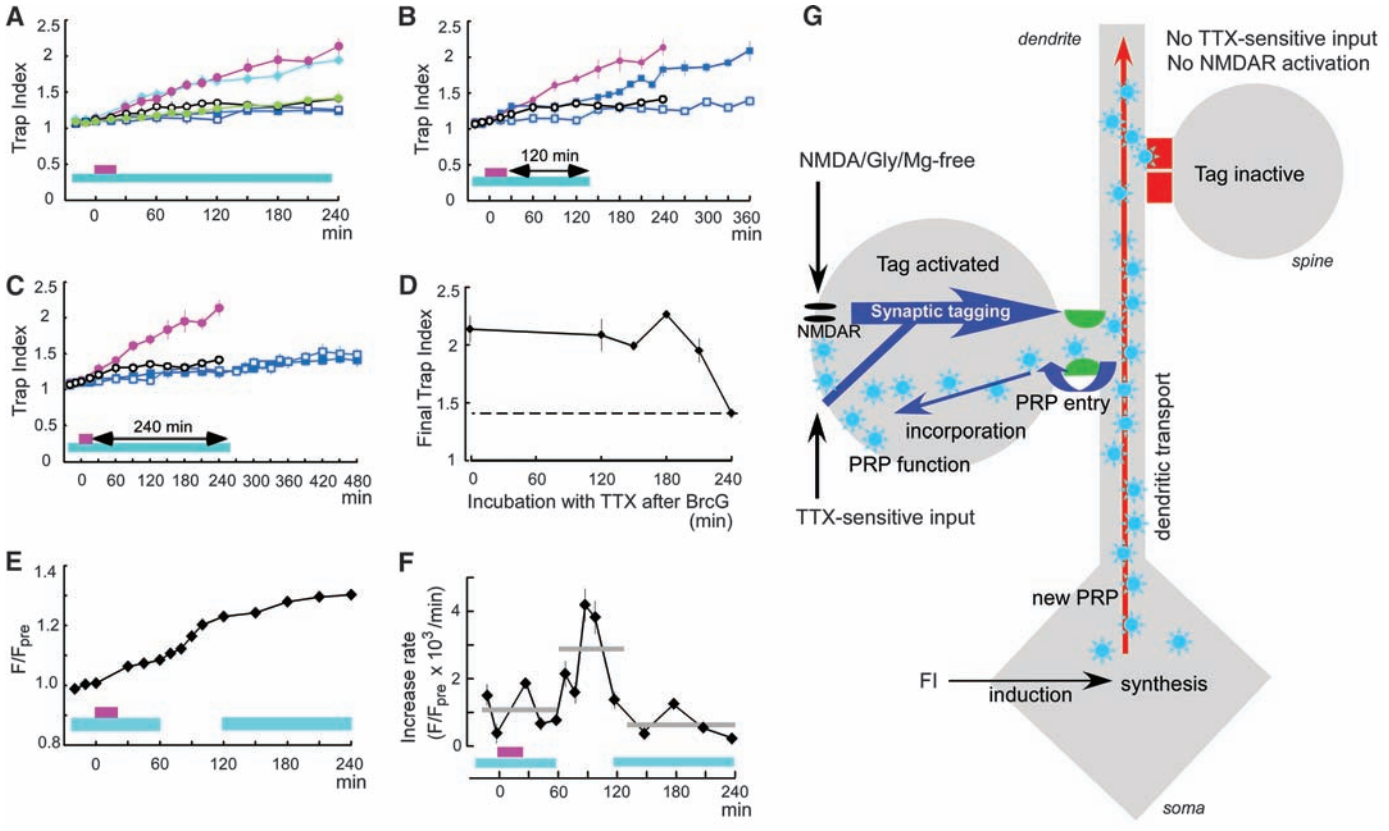

Fig. 6. Persistent activation of PKG signaling. (**A**) Trap index time courses. Solid magenta circles, BrcG on VE; solid green circles, BrcG on EGFP; solid cyan diamonds, BrcG + 50 nM TTX; solid blue squares, BrcG + 1 μM TTX; open blue squares, 1 μM TTX alone; open circles, ACSF alone. Vertical bars, SEM; horizontal bars, application of BrcG (magenta) and TTX (blue). (**B**) Neurons were stimulated with BrcG in the presence of 1 μM TTX. TTX application was continued for an additional 2 hours, then TTX was washed out for 4 hours. Symbols are as in (A). (**C**) Experiment with longer (4 hours) TTX incubation. Symbols are as in (A). (**D**) Trap index 4 hours after TTX cessation versus TTX incubation time. (**E**) F/F_{pre} time-course analysis showing that TTX application blocked VE trapping, which was recovered during washout. (**F**) The time-course analysis of the increase rates (F/F_{pre} change per time interval). Horizontal gray bars indicate the averages of increase rates during the different periods (first TTX incubation, washout, and second TTX incubation). (E) and (F) depict averages and SEM (vertical bars) from 2234 spines of eight cells. (**G**) Summary diagram showing somatically synthesized new PRPs (solar symbols), among which Vesl-1S is carried by microtubule-based vesicular transport along dendrites. Vesl-1S in the dendrites cannot enter spines without specific inputs (red closed gate in the distal spine neck). A synaptic tag successfully comes into operation exclusively in spines that receive both NMDA receptor activation and the TTX-sensitive input, which releases the blockade against Vesl-1S entry into spines (green open gate in the spine neck).

contribute to late-phase plasticity. The preferred mechanism for PRP trapping would thus involve transfer of the PRP from the kinesin-dependent dendritic transport to the myosin V–dependent intraspine transport. Interaction of myosin V with GluR1-containing recycling vesicles through rab11-FIP2 (*36*) has been reported, as well as direct interaction of myosin V with the C-terminal region of GluR1 (*22*, *37*).

References and Notes

1. K. G. Reymann, J. U. Frey, *Neuropharmacology* **52**, 24 (2007).
2. U. Frey, R. G. M. Morris, *Nature* **385**, 533 (1997).
3. K. C. Martin *et al.*, *Cell* **91**, 927 (1997).
4. K. C. Martin, K. S. Kosik, *Nat. Rev. Neurosci.* **3**, 813 (2002).
5. O. Steward, C. S. Wallace, G. L. Lyford, P. F. Worley, *Neuron* **21**, 741 (1998).
6. I. A. Muslimov *et al.*, *J. Biol. Chem.* **279**, 52613 (2004).
7. W. Ju *et al.*, *Nat. Neurosci.* **7**, 244 (2004).
8. W. Smith, S. Starck, R. Roberts, E. Schuman, *Neuron* **45**, 765 (2005).
9. N. Matsuo, L. Reijmers, M. Mayford, *Science* **319**, 1104 (2008).
10. U. Frey, R. G. M. Morris, *Trends Neurosci.* **21**, 181 (1998).
11. A. Barco, J. M. Alarcon, E. R. Kandel, *Cell* **108**, 689 (2002).
12. R. Fonseca, U. V. Nägerl, R. G. M. Morris, T. Bonhoeffer, *Neuron* **44**, 1011 (2004).
13. B. L. Bloodgood, B. L. Sabatini, *Science* **310**, 866 (2005).
14. N. Honkura, M. Matsuzaki, J. Noguchi, G. C. R. Ellis-Davis, H. Kasai, *Neuron* **57**, 719 (2008).
15. K. Shen, T. Meyer, *Science* **284**, 162 (1999).
16. M. Ackermann, A. Matus, *Nat. Neurosci.* **6**, 1194 (2003).
17. X. P. Ryan *et al.*, *Neuron* **47**, 85 (2005).
18. U. Frey, R. G. M. Morris, *Neuropharmacology* **37**, 545 (1998).
19. A. Kato, F. Ozawa, Y. Saitoh, K. Hirai, K. Inokuchi, *FEBS Lett.* **412**, 183 (1997).
20. P. R. Brakeman *et al.*, *Nature* **386**, 284 (1997).
21. N. Inoue *et al.*, *Mol. Brain* **2**, 10.1186/1756-6606-2-7 (2009).
22. See supporting material on *Science* Online.
23. R. Okubo-Suzuki, D. Okada, M. Sekiguchi, K. Inokuchi, *Mol. Cell. Neurosci.* **38**, 266 (2008).
24. G. E. Hardingham, Y. Fukunaga, H. Bading, *Nat. Neurosci.* **5**, 405 (2002).
25. M. Matsuzaki, N. Honkura, G. C. R. Ellis-Davies, H. Kasai, *Nature* **429**, 761 (2004).
26. H. Ageta *et al.*, *J. Biol. Chem.* **276**, 15893 (2001).
27. Y. Niibori, F. Hayashi, K. Hirai, M. Matsui, K. Inokuchi, *Neurosci. Res.* **57**, 399 (2007).
28. F. Ango *et al.*, *J. Neurosci.* **20**, 8710 (2000).
29. A. Kato *et al.*, *J. Biol. Chem.* **273**, 23969 (1998).
30. G. H. Patterson, J. Lippincott-Schwartz, *Science* **297**, 1873 (2002).
31. B. Xiao *et al.*, *Neuron* **21**, 707 (1998).
32. K. S. Christopherson, B. J. Hillier, W. A. Lim, D. S. Bredt, *J. Biol. Chem.* **274**, 27467 (1999).
33. H. G. Wang *et al.*, *Neuron* **45**, 389 (2005).
34. P. J. Mackenzie, T. H. Murphy, *J. Neurophysiol.* **80**, 2089 (1998).
35. J. C. Magee, M. Carruth, *J. Neurophysiol.* **82**, 1895 (1999).
36. Z. Wang *et al.*, *Cell* **135**, 535 (2008).
37. S. S. Correia *et al.*, *Nat. Neurosci.* **11**, 457 (2008).

38. We thank A. Miyawaki (RIKEN, Japan) for the gift of PAGFP. Supported partly by grants from the Ministry of Education, Technology and Culture (K.I.), the Special Coordinate Funds for Promoting Science and Technology from MEXT of the Japanese Government (K.I.), and JST-CREST (K.I.).

Supporting Online Material

www.sciencemag.org/cgi/content/full/324/5929/904/DC1
Materials and Methods
SOM Text
Figs. S1 to S10
Tables S1 to S3
References and Notes

27 January 2009; accepted 2 April 2009
10.1126/science.1171498